ACS APPLIED MATERIALS & INTERFACES

Research Article

Cite This: ACS Appl. Mater. Interfaces 2017, 9, 44579−44583

www.acsami.org

Highly Efficient Broadband Yellow Phosphor Based on Zero-Dimensional Tin Mixed-Halide Perovskite

Chenkun Zhou,[†,#] Yu Tian,[‡,#] Zhao Yuan,[†] Haoran Lin,[†] Banghao Chen,[§] Ronald Clark,[§] Tristan Dilbeck,[§] Yan Zhou,[§] Joseph Hurley,[§] Jennifer Neu,[†,∥] Tiglet Besara,[†,∥] Theo Siegrist,[†,∥] Peter Djurovich,[⊥] and Biwu Ma*[,†,‡,§]

[†]Department of Chemical and Biomedical Engineering, FAMU-FSU College of Engineering, Tallahassee, Florida 32310, United States

[‡]Materials Science and Engineering Program and [§]Department of Chemistry and Biochemistry, Florida State University, Tallahassee, Florida 32306, United States

[∥]National High Magnetic Field Laboratory, Florida State University, Tallahassee, Florida 32310, United States

[⊥]Department of Chemistry, University of Southern California, Los Angeles, California 90089, United States

Supporting Information

ABSTRACT: Organic−inorganic hybrid metal halide perovskites have emerged as a highly promising class of light emitters, which can be used as phosphors for optically pumped white light-emitting diodes (WLEDs). By controlling the structural dimensionality, metal halide perovskites can exhibit tunable narrow and broadband emissions from the free-exciton and self-trapped excited states, respectively. Here, we report a highly efficient broadband yellow light emitter based on zero-dimensional tin mixed-halide perovskite $(C_4N_2H_{14}Br)_4SnBr_xI_{6-x}$ (x = 3). This rare-earth-free ionically bonded crystalline material possesses a perfect host-dopant structure, in which the light-emitting metal halide species ($SnBr_xI_{6-x}^{4-}$, x = 3) are completely isolated from each other and embedded in the wide band gap organic matrix composed of $C_4N_2H_{14}Br^-$. The strongly Stokes-shifted broadband yellow emission that peaked at 582 nm from this phosphor, which is a result of excited state structural reorganization, has an extremely large full width at half-maximum of 126 nm and a high photoluminescence quantum efficiency of ∼85% at room temperature. UV-pumped WLEDs fabricated using this yellow emitter together with a commercial europium-doped barium magnesium aluminate blue phosphor ($BaMgAl_{10}O_{17}:Eu^{2+}$) can exhibit high color rendering indexes of up to 85.

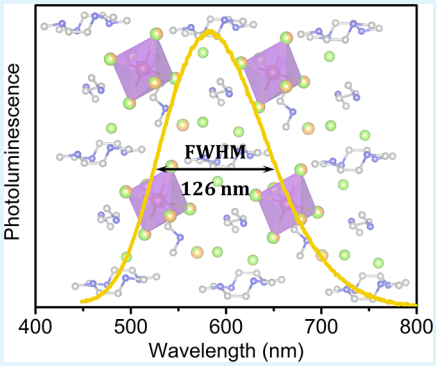

KEYWORDS: *perovskite, lead-free, 0D structure, yellow phosphor, white LEDs*

INTRODUCTION

Solid-state lighting (SSL) has been steadily changing the way we light our homes, businesses, and cities over the last decade because of its low energy consumption, high efficiency, and long lifetime as compared to conventional incandescent and fluorescent light sources.[1,2] To mimic the blackbody radiation of an incandescent bulb (or white emission), typical SSL devices consist of light-emitting diodes (LEDs) coated with a single phosphor [for instance, a blue LED (InGaN) coated with a yellow phosphor (cerium-doped yttrium aluminum garnet, YAG:Ce^{3+})] or a mixture of phosphors (for instance, an ultraviolet LED coated with blue and yellow phosphors).[3−6] Despite remarkable advances in down-conversion white light-emitting diodes (WLEDs), a number of issues and challenges remain to be resolved to further improve the device performance and reduce the cost. For instance, YAG:Ce^{3+}-based WLEDs usually have poor color rendering indexes (CRIs) and high correlated color temperatures (CCTs) because of the deficiency in the red emission of YAG:Ce^{3+}.[7,8] Adding a narrow-band red-emitting phosphor to the YAG:Ce^{3+}-based WLEDs can significantly improve the color quality,[9] but it complicates the device fabrication with increased cost. The same issue of limited coverage of the full visible spectrum presents in UV-pumped WLEDs using mixtures of blue and yellow phosphors.[10] Developing broadband yellow phosphors with a large full width at half-maximum (fwhm) is an effective approach to addressing this issue. Another challenge for down-conversion WLEDs is that almost all the commercial phosphors contain rare-earth elements, for example, europium, cerium, terbium, and yttrium.[11] As the demand for rare earth elements continues to increase in almost all high-tech applications, their potential supply risks and raised prices make the search for alternative rare-earth-free phosphors significantly important.[12]

Hybrid organic−inorganic metal halide perovskites have recently emerged as a highly promising class of light-emitting materials with excellent color tunability and high photo-

Received: August 25, 2017
Accepted: December 5, 2017
Published: December 5, 2017

DOI: 10.1021/acsami.7b12862
ACS Appl. Mater. Interfaces 2017, 9, 44579−44583

luminescence quantum efficiency (PLQE). Tunable narrow-band emission has been realized in 2D, quasi-2D, and 3D perovskites as a result of radiative decay from the free-exciton excited states.[13−16] Broadband emission has been observed in corrugated-2D, 1D, and 0D perovskites as a result of efficient exciton self-trapping (or excited state structural reorganization) in the quantum-confined structures.[17−22] Recently, we reported a broadband yellow emitting zero-dimensional (0D) lead-free tin bromide perovskite $(C_4N_2H_{14}Br)_4SnBr_6$ (peaked at 570 nm) with an fwhm of 105 nm and a near-unity PLQE.[22,23] A UV-pumped WLED using this 0D tin bromide perovskite as a yellow phosphor was fabricated that had a CRI of around 70, a value still not ideal for indoor lighting because of the deficiency in red emission.

Here, we report a new 0D tin mixed-halide perovskite with a much broader yellow emission than that of $(C_4N_2H_{14}Br)_4SnBr_6$. By incorporating both bromide and iodide in the metal halide octahedron, a single crystalline 0D tin mixed-halide perovskite $(C_4N_2H_{14}Br)_4SnBr_xI_{6-x}$ (x = 3) has been prepared that shows a slightly red-shift broadband yellow emission (peaked at 582 nm) with a large fwhm of 126 nm and a PLQE of ∼85%. UV-pumped LEDs have been fabricated using this new yellow phosphor blended with a blue phosphor ($BaMgAl_{10}O_{17}:Eu^{2+}$). A high CRI of 85 was achieved for a WLED because of the extended emission of this yellow phosphor into the red visible region.

RESULTS AND DISCUSSIONS

The 0D Sn mixed-halide perovskite single crystals were prepared by means of antisolvent vapor crystallization in a high yield (∼60%),[22] that is, slowly diffusing dichloromethane into a precursor solution of Sn halide (SnX_2, X = Br, I) and *N*,*N*′-dimethylethylene-1,2-diammonium halide salt ($C_4N_2H_{14}X_2$, X = Br, I) in dimethylformamide (DMF) at room temperature. This process was carried out in an N_2-filled glovebox to prevent the oxidation of SnX_2. The exact composition of bulk single crystals was found to be different from the stoichiometry of precursor solutions for the mixed-halide perovskite because of the higher solubility of iodide salts in DMF than that of bromide ones. The crystal structure of the 0D Sn mixed-halide perovskite was determined using single-crystal X-ray diffraction (SCXRD), as shown in Figure 1. The mixed-halide perovskite adopts the same triclinic space group ($P\bar{1}$) as that of previously reported 0D pure-halide perovskites,

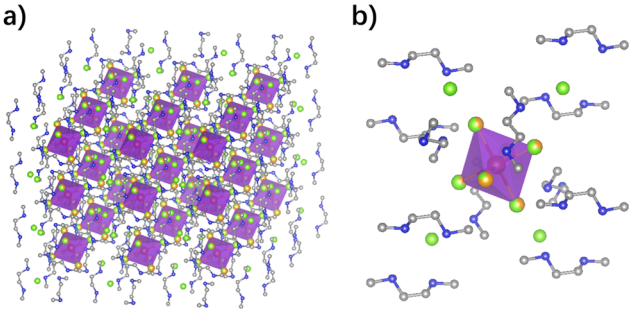

Figure 1. (a) Single-crystal structure of the Sn mixed-halide perovskite $(C_4N_2H_{14}Br)_4SnBr_xI_{6-x}$ (x = 3) (red spheres: tin atoms; green spheres: bromine atoms; orange spheres: iodine atoms; blue spheres: nitrogen atoms; and gray spheres: carbon atoms; hydrogen atoms were hidden for clarity). (b) Individual Sn mixed-halide octahedron completely surrounded by organic ligands.

with isolated metal halide octahedrons (Figure 1a) surrounded by the organic ligands (Figure 1b). The average Sn−X bond distance (3.113 Å) is determined to be slightly longer than that of its bromide counterpart $(C_4N_2H_{14}Br)_4SnBr_6$ (3.052 Å) and shorter than that of its iodide counterpart $(C_4N_2H_{14}I)_4SnI_6$ (3.219 Å). The octahedral SnX_6^{4-} contains equal amounts of bromine and iodine, whereas all the four halide ions associated with the organic ligand are bromines, resulting in a chemical formula of $(C_4N_2H_{14}Br)_4SnBr_xI_{6-x}$ (x = 3). The crystal diffraction data are summarized in Table S1. The powder X-ray diffraction pattern of hand-milled bulk crystal powders displays exactly the same features as the simulated pattern from SCXRD, suggesting a uniform crystal structure of as-synthesized bulk crystals (Figure S1). Elemental analysis was also used to characterize the bulk perovskite crystals, in which bromine and iodine analyses were performed by flask combustion followed by ion chromatography. The chemical formula obtained by element analysis is consistent with that determined by SCXRD, $(C_4N_2H_{14}Br)_4SnBr_xI_{6-x}$ (x = 3), which also confirmed the purity and uniformity of the bulk 0D Sn mixed-halide perovskite crystals.

To further verify the chemical structure of $(C_4N_2H_{14}Br)_4SnBr_xI_{6-x}$ (x = 3) for the 0D Sn mixed-halide perovskite crystals, we have recorded the ^{119}Sn magic-angle spinning (MAS) nuclear magnetic resonance (NMR) spectroscopy spectra for the mixed-halide sample, as well as 0D

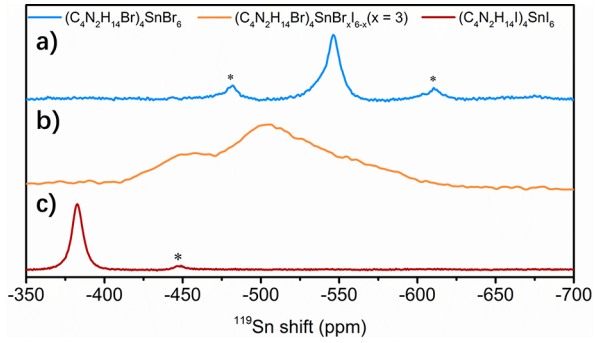

Figure 2. ^{119}Sn MAS NMR spectra of $(C_4N_2H_{14}Br)_4SnBr_6$ (a), $(C_4N_2H_{14}Br)_4SnBr_xI_{6-x}$ (x = 3) (b), and $(C_4N_2H_{14}I)_4SnI_6$ (c), recorded at room temperature spinning at 12 kHz. Spinning sidebands are indicated with asterisks.

$(C_4N_2H_{14}Br)_4SnBr_6$ and $(C_4N_2H_{14}I)_4SnI_6$. Figure 2 shows the ^{119}Sn MAS NMR spectra of all three samples. Both 0D $(C_4N_2H_{14}Br)_4SnBr_6$ and $(C_4N_2H_{14}I)_4SnI_6$ exhibit only one tin site at −546.8 and −382.2 ppm, which is in agreement with the crystal structure and shielding features. For the mixed-halide sample, a broad resonance was observed with two maximums at −456 and −504 ppm, which is likely because of the presence of two isomers (facial and meridional) in the 0D $(C_4N_2H_{14}Br)_4SnBr_xI_{6-x}$ (x = 3). These experimental results are consistent with the calculation results using the Cambridge Serial Total Energy Package (CASTEP).

Photophysical properties of the bulk perovskite crystals were investigated using UV−vis absorption spectroscopy (Figure S2), as well as steady-state and time-resolved emission spectroscopies. Figure 3a shows the images of the bulk crystals under ambient light and UV light (365 nm). The yellowish chunk-shape crystals were highly emissive under UV illumination. Figure 3b shows the excitation and emission spectra of the

DOI: 10.1021/acsami.7b12862
ACS Appl. Mater. Interfaces 2017, 9, 44579−44583

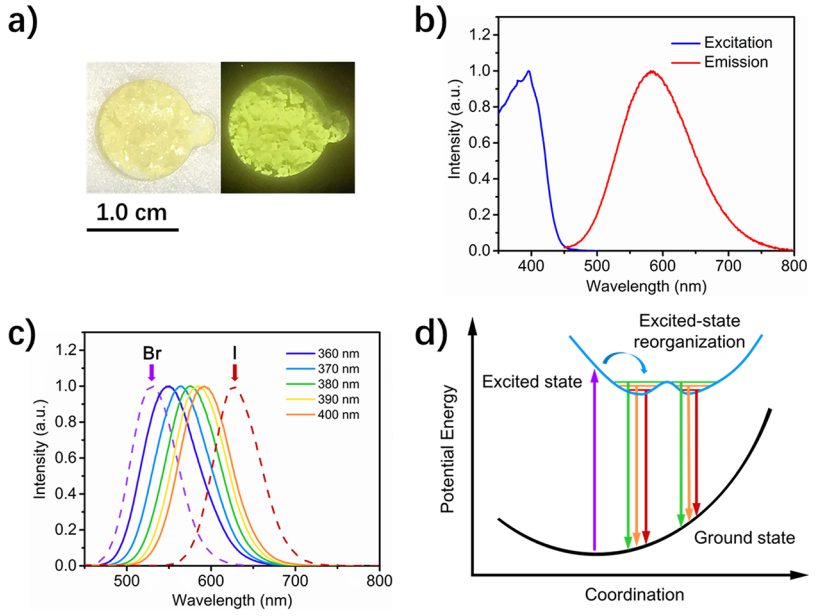

Figure 3. (a) Photo images of bulk Sn mixed-halide perovskite crystals under ambient light and a UV-lamp irradiation (365 nm). (b) Excitation (blue line) and emission (red line) spectra of bulk Sn mixed-halide perovskite crystals at room temperature. (c) Emission spectra of $(C_4N_2H_{14}Br)_4SnBr_xI_{6-x}$ ($x = 3$) excited at different wavelength (360–400 nm), $(C_4N_2H_{14}Br)_4SnBr_6$ (dash line, purple), and $(C_4N_2H_{14}I)_4SnI_6$ (dash line, red) at 77 K. (d) Schematic of the potential energy curves of mixed-halide perovskite crystals in a configuration space.

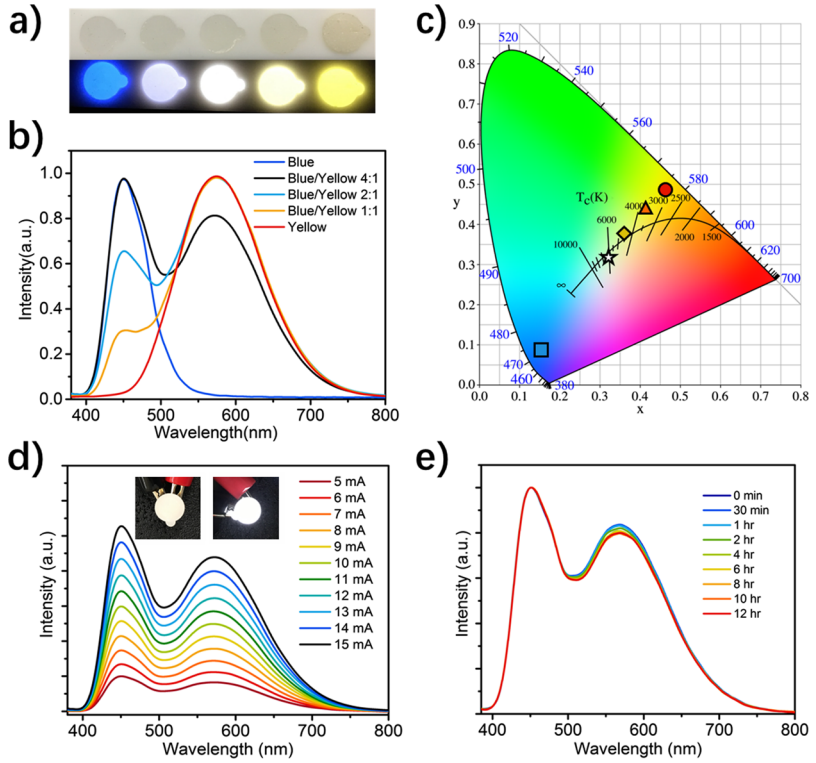

Figure 4. 0D Sn mixed-halide perovskite $(C_4N_2H_{14}Br)_4SnBr_xI_{6-x}$ ($x = 3$) as a yellow phosphor for UV-pumped WLEDs. (a) Images of blue and yellow phosphors with different weight ratios (from left to right, 1:0, 4:1, 2:1, 1:1, and 0:1) embedded in PDMS under ambient light (top) and UV light (bottom). (b) Emission spectra of UV-pumped LEDs with different blue and yellow phosphor weight ratios. (c) CIE coordinates and CCTs for the UV-pumped LEDs plotted on the CIE1931 color space chromaticity chart: blue (■), white (★), "warm" whites (◆), and (▲), and yellow (●). (d) Emission spectra of a "cold" WLED at different driving currents; the inset shows the devices off and on. (e) Emission stability of a WLED at 10 mA driving current for 12 h.

bulk crystals. Red shifts in the excitation (from 355 to 395 nm) and emission (from 570 to 582 nm) maxima are observed for $(C_4N_2H_{14}Br)_4SnBr_xI_{6-x}$ ($x = 3$), as compared to $(C_4N_2H_{14}Br)_4SnBr_6$. The bathochromic shifts are consistent with the weaker ligand field strength of iodide versus bromide ions. Similar to the previously reported Sn pure-halide perovskites, this mixed-halide perovskite also displays a large Stokes shift of 187 nm. An fwhm of 126 nm is recorded in

DOI: 10.1021/acsami.7b12862
ACS Appl. Mater. Interfaces 2017, 9, 44579–44583

$(C_4N_2H_{14}Br)_4SnBr_xI_{6-x}$ ($x = 3$), which is much larger than that of $(C_4N_2H_{14}Br)_4SnBr_6$ (105 nm). The red-shifted emission spectrum and large fwhm suggest that $(C_4N_2H_{14}Br)_4SnBr_xI_{6-x}$ ($x = 3$) could be a better suited yellow phosphor for UV-pumped WLEDs than $(C_4N_2H_{14}Br)_4SnBr_6$. The luminescence decay lifetime of the bulk crystals at room temperature is around 0.7 μs (Figure S3), which is close to those of its pure-halide counterparts. The PLQE of this 0D Sn mixed-halide perovskite was measured at ~85% at room temperature (Figure S4). It is worthwhile to point out that this mixed-halide perovskite displayed an excellent photo- and thermo-stability, even higher than its pure-halide counterparts (Figure S5). Unlike typical 3D and 2D mixed-halide perovskites with efficient ion exchanges, this 0D structure with the metal mixed-halide octahedrons completely isolated from each other and surrounded by organic ligands could have significantly reduced ion diffusion, leading to much higher photostability. Thermogravimetric analysis shows that the Sn mixed-halide perovskite does not decompose until 260 °C (Figure S6). Also, the emission intensity decreases without the change of the spectral shape upon the increase of temperature from room temperature to 80 °C, which is likely because of the enhanced nonradiative decay. The emission intensity recovers after cooling from 80 °C to room temperature, suggesting a very good thermo-stability of this 0D mix-halide perovskite material (Figure S7).

Interestingly, the emission spectra of 0D $(C_4N_2H_{14}Br)_4SnBr_xI_{6-x}$ ($x = 3$) are dependent on excitation energy at 77 K, undergoing red shift upon the increasing of excitation wavelength (Figure 3c). The luminescence decay lifetimes also change slightly for different emissions (Figure S8). Such an excitation-dependent photoluminescence phenomenon is not observed in 0D pure-halide perovskites $(C_4N_2H_{14}Br)_4SnBr_6$ and $(C_4N_2H_{14}I)_4SnI_6$, of which emissions are independent of excitation energy. The excitation dependence is likely due to the multiexcited states in the mixed-halide perovskite, as shown in Figure 3d. Unlike pure-halide perovskites with one energy minimum as a result of the structural reorganization of pure metal halide emissive species $SnBr_6^{4-}$ or SnI_6^{4-}, the mixed-halide perovskite could form two or more energy minima as a result of structural distortion of either Sn−Br or Sn−I upon photoexcitation depending on the excitation wavelength. At room temperature, excitons located in two energy minima could reach thermally activated equilibrium, resulting in excitation-independent emissions that are broader than those of pure-halide perovskites. However, at 77 K with little-to-no thermally activated equilibrium, the overall emission spectrum is a combination of decays from different excitation-dependent distorted structures (Figure 3d).

The application of this 0D $(C_4N_2H_{14}Br)_4SnBr_xI_{6-x}$ ($x = 3$) as a broadband yellow phosphor in optically pumped LEDs was investigated. Several down-conversion phosphor composites were prepared by blending this yellow phosphor with a commercial blue phosphor $Ba_{0.86}Eu_{0.14}MgAl_{10}O_{17}$ at different weight ratios (1:0, 4:1, 2:1, 1:1, and 0:1) in polydimethylsiloxane (PDMS) matrix. Thin films of the phosphor-doped PDMS are almost colorless under ambient light but show strong luminescence with blue, white, and yellow colors under UV illumination (Figure 4a). To construct optically pumped LEDs, a commercial UV LED (340 nm) was chosen as a light source, considering both yellow and blue phosphors have excitations in the UV-light region. Figure 4b shows the emission spectra of UV-pumped LEDs, in which the phosphor-doped PDMS films were attached to the commercial UV LED. The Commission Internationale de l'Eclairage (CIE) color coordinates, CCTs, and CRIs of the UV-pumped LEDs are summarized in Table 1.

Table 1. CIE Coordinates, CCTs, and CRIs of UV-Pumped LEDs with Different Blue to Yellow Phosphor Weight Ratios

blue/yellow	CIE (x, y)	CCT/K	CRI
1:0	(0.15, 0.09)	N/A	N/A
4:1	(0.32, 0.32)	6160	84
2:1	(0.36, 0.38)	4600	85
1:1	(0.41, 0.44)	3740	78
0:1	(0.46, 0.49)	3200	67

Figure 4c shows the plots of the CIE color coordinates and CCTs of the light emissions on the CIE1931 color space chromaticity chart. White light ranging from "cold" to "warm" is achieved by simply varying the ratio of blue and yellow phosphors. A near-perfect white emission with CIE coordinates of (0.32, 0.32) and a CCT value of 6160 K has been obtained with the weight ratio of blue to yellow phosphor at 4 to 1. This white emission has a CRI of 84, which is much higher than that of conventional WLEDs based on the YAG:Ce^{3+} yellow phosphor coupled with a blue LED[8] and $(C_4N_2H_{14}Br)_4SnBr_6$-based WLEDs of around 70. The high CRI is due to the fact that $(C_4N_2H_{14}Br)_4SnBr_xI_{6-x}$ ($x = 3$) has a broader emission with better coverage in the red region than YAG:Ce^{3+} and $(C_4N_2H_{14}Br)_4SnBr_6$. Excellent color stability has been observed in the UV-pumped LEDs at different driving currents, as shown in Figure 4d. The high color stability can be attributed to minimal energy transfer from the blue phosphor to the yellow phosphor because there is a little-to-no overlap between the excitations of the yellow phosphor and the emission of the blue phosphor. The UV-pumped LEDs also showed good stability in air (relative humidity ≈ 35%) with minimal change in the emission color during the operation for more than 12 h under the 10 mA driving current, as shown in Figure 4e.

CONCLUSIONS

In summary, we have designed and synthesized a novel rare-earth free broadband yellow phosphor based on the 0D tin mixed-halide perovskite $(C_4N_2H_{14}Br)_4SnBr_xI_{6-x}$ ($x = 3$), which has a high quantum efficiency of ~85% and excellent photostability at room temperature. The emission band of this 0D mixed-halide perovskite is broader than those of its pure-halide counterparts because of the multiexcited states created by the structural reorganization of the metal mixed-halide octahedrons. By overcoming the issue of deficiency in the red emission present in most yellow phosphors, this 0D tin mixed-halide perovskite enabled optically pumped WLEDs with high CRIs of up to 85. Considering the low cost of eco-friendly raw materials, room-temperature facile synthesis, and excellent optical properties, this new perovskite phosphor represents a highly promising alternative to replace conventional inorganic rare-earth-based phosphors and quantum dot-based phosphors that currently dominate the field of optically pumped WLEDs.

ASSOCIATED CONTENT

Supporting Information

The Supporting Information is available free of charge on the ACS Publications website at DOI: 10.1021/acsami.7b12862.

Syntheses and characterizations of the 0D bulk tin mixed-halide perovskite crystals and results, as well as the

DOI: 10.1021/acsami.7b12862
ACS Appl. Mater. Interfaces 2017, 9, 44579−44583

preparation process of phosphors in white LED demo (PDF)
Crystallographic data (CIF)

AUTHOR INFORMATION

Corresponding Author

*E-mail: bma@fsu.edu.

ORCID

Zhao Yuan: 0000-0003-3799-489X
Tiglet Besara: 0000-0002-2143-2254
Biwu Ma: 0000-0003-1573-8019

Author Contributions

#C.Z. and Y.T. contributed equally.

Notes

The authors declare no competing financial interest.

ACKNOWLEDGMENTS

The authors acknowledge the Florida State University (FSU) for financial support through the Energy and Materials Initiative and GAP Commercialization Grant Program. FSU and National Science Foundation (NSF) Major Research Instrumentation (MRI) program (NSF 1126587) are appreciated for the support of the upgrades to the solid-state NMR facility. The authors also thank Dr. Hanwei Gao for providing access to the instrument for photostability test, Dr. Victor Terskikh and Canada National Ultrahigh-Field NMR Facility for access to CASTEP software.

REFERENCES

(1) Žukauskas, A.; Shur, M. S.; Gaska, R. Light-Emitting Diodes: Progress in Solid-State Lighting. *MRS Bull.* **2001**, *26*, 764−769.
(2) De Almeida, A.; Santos, B.; Paolo, B.; Quicheron, M. Solid State Lighting Review—Potential and Challenges in Europe. *Renewable Sustainable Energy Rev.* **2014**, *34*, 30−48.
(3) McKittrick, J.; Shea-Rohwer, L. E. Review: Down Conversion Materials for Solid-State Lighting. *J. Am. Ceram. Soc.* **2014**, *97*, 1327−1352.
(4) Lin, C. C.; Liu, R.-S. Advances in Phosphors for Light-Emitting Diodes. *J. Phys. Chem. Lett.* **2011**, *2*, 1268−1277.
(5) Roushan, M.; Zhang, X.; Li, J. Solution-Processable White-Light-Emitting Hybrid Semiconductor Bulk Materials with High Photoluminescence Quantum Efficiency. *Angew. Chem., Int. Ed.* **2012**, *51*, 436−439.
(6) Haranath, D.; Chander, H.; Sharma, P.; Singh, S. Enhanced Luminescence of $Y_3Al_5O_{12}:Ce^{3+}$ Nanophosphor for White Light-Emitting Diodes. *Appl. Phys. Lett.* **2006**, *89*, 173118.
(7) Shang, M.; Li, G.; Geng, D.; Yang, D.; Kang, X.; Zhang, Y.; Lian, H.; Lin, J. Blue Emitting $Ca_8La_2(PO_4)_6O_2:Ce^{3+}/Eu^{2+}$ Phosphors with High Color Purity and Brightness for White LED: Soft-Chemical Synthesis, Luminescence, and Energy Transfer Properties. *J. Phys. Chem. C* **2012**, *116*, 10222−10231.
(8) Pimputkar, S.; Speck, J. S.; DenBaars, S. P.; Nakamura, S. Prospects for LED Lighting. *Nat. Photonics* **2009**, *3*, 180−182.
(9) Pust, P.; Weiler, V.; Hecht, C.; Tücks, A.; Wochnik, A. S.; Henß, A.-K.; Wiechert, D.; Scheu, C.; Schmidt, P. J.; Schnick, W. Narrow-Band Red-Emitting $Sr[LiAl_3N_4]:Eu^{2+}$ as a Next-Generation LED-Phosphor Material. *Nat. Mater.* **2014**, *13*, 891−896.
(10) Park, S.-I.; Xiong, Y.; Kim, R.-H.; Elvikis, P.; Meitl, M.; Kim, D.-H.; Wu, J.; Yoon, J.; Yu, C.-J.; Liu, Z.; Huang, Y.; Hwang, K.-c.; Ferreira, P.; Li, X.; Choquette, K.; Rogers, J. A. Printed Assemblies of Inorganic Light-Emitting Diodes for Deformable and Semitransparent Displays. *Science* **2009**, *325*, 977−981.
(11) Xie, R.-J.; Hirosaki, N.; Sakuma, K.; Yamamoto, Y.; Mitomo, M. Eu^{2+}-Doped Ca-α-SiAlON: A Yellow Phosphor for White Light-Emitting Diodes. *Appl. Phys. Lett.* **2004**, *84*, 5404−5406.
(12) Bauer, D.; Diamond, D.; Li, J.; McKittrick, M.; Sandalow, D.; Telleen, P. *US Department of Energy Critical Materials Strategy*, 2011.
(13) Protesescu, L.; Yakunin, S.; Bodnarchuk, M. I.; Krieg, F.; Caputo, R.; Hendon, C. H.; Yang, R. X.; Walsh, A.; Kovalenko, M. V. Nanocrystals of Cesium Lead Halide Perovskites ($CsPbX_3$, X = Cl, Br, and I): Novel Optoelectronic Materials Showing Bright Emission with Wide Color Gamut. *Nano Lett.* **2015**, *15*, 3692−3696.
(14) Sichert, J. A.; Tong, Y.; Mutz, N.; Vollmer, M.; Fischer, S.; Milowska, K. Z.; Cortadella, R. G.; Nickel, B.; Cardenas-Daw, C.; Stolarczyk, J. K.; Urban, A. S.; Feldmann, J. Quantum Size Effect in Organometal Halide Perovskite Nanoplatelets. *Nano Lett.* **2015**, *15*, 6521−6527.
(15) Dou, L.; Wong, A. B.; Yu, Y.; Lai, M.; Kornienko, N.; Eaton, S. W.; Fu, A.; Bischak, C. G.; Ma, J.; Ding, T.; Ginsberg, N. S.; Wang, L.-W.; Alivisatos, A. P.; Yang, P. Atomically Thin Two-Dimensional Organic-Inorganic Hybrid Perovskites. *Science* **2015**, *349*, 1518−1521.
(16) Yuan, Z.; Shu, Y.; Xin, Y.; Ma, B. Highly Luminescent Nanoscale Quasi-2D Layered Lead Bromide Perovskites with Tunable Emissions. *Chem. Commun.* **2016**, *52*, 3887−3890.
(17) Dohner, E. R.; Hoke, E. T.; Karunadasa, H. I. Self-Assembly of Broadband White-Light Emitters. *J. Am. Chem. Soc.* **2014**, *136*, 1718−1721.
(18) Dohner, E. R.; Jaffe, A.; Bradshaw, L. R.; Karunadasa, H. I. Intrinsic White-Light Emission from Layered Hybrid Perovskites. *J. Am. Chem. Soc.* **2014**, *136*, 13154−13157.
(19) Hu, T.; Smith, M. D.; Dohner, E. R.; Sher, M.-J.; Wu, X.; Trinh, M. T.; Fisher, A.; Corbett, J.; Zhu, X.-Y.; Karunadasa, H. I.; Lindenberg, A. M. Mechanism for Broadband White-Light Emission from Two-Dimensional (110) Hybrid Perovskites. *J. Phys. Chem. Lett.* **2016**, *7*, 2258−2263.
(20) Cortecchia, D.; Yin, J.; Bruno, A.; Lo, S.-Z. A.; Gurzadyan, G. G.; Mhaisalkar, S.; Bredas, J.-L.; Soci, C. Polaron Self-Localization in White-Light Emitting Hybrid Perovskites. *J. Mater. Chem. C* **2017**, *5*, 2771−2780.
(21) Yuan, Z.; Zhou, C.; Tian, Y.; Shu, Y.; Messier, J.; Wang, J. C.; van de Burgt, L. J.; Kountouriotis, K.; Xin, Y.; Holt, E.; Schanze, K.; Clark, R.; Siegrist, T.; Ma, B. One-Dimensional Organic Lead Halide Perovskites with Efficient Bluish White-Light Emission. *Nat. Commun.* **2017**, *8*, 14051.
(22) Zhou, C.; Lin, H.; Tian, Y.; Yuan, Z.; Clark, R.; Chen, B.; van de Burgt, L. J.; Wang, J. C.; Zhou, Y.; Hanson, K.; Meisner, Q. J.; Neu, J.; Besara, T.; Siegrist, T.; Lambers, E.; Djurovich, P.; Ma, B. Luminescent Zero-Dimensional Organic Metal Halide Hybrids with Near-Unity Quantum Efficiency. *Chem. Sci.* **2018**, DOI: 10.1039/C7SC04539E.
(23) Zhou, C.; Tian, Y.; Wang, M.; Rose, A.; Besara, T.; Doyle, N. K.; Yuan, Z.; Wang, J. C.; Clark, R.; Hu, Y.; Siegrist, T.; Lin, S.; Ma, B. Low-Dimensional Organic Tin Bromide Perovskites and Their Photoinduced Structural Transformation. *Angew. Chem., Int. Ed.* **2017**, *56*, 9018−9022.

DOI: 10.1021/acsami.7b12862
ACS Appl. Mater. Interfaces 2017, 9, 44579−44583